Scripta Materialia 201 (2021) 113975

Contents lists available at ScienceDirect

Scripta Materialia

journal homepage: www.elsevier.com/locate/scriptamat

Work hardening discrepancy designing to strengthening gradient nanotwinned Cu

Tao Wan[a,b,1], Zhao Cheng[a,1], Linfeng Bu[a,c], Lei Lu[a,2,*]

[a] Shenyang National Laboratory for Materials Science, Institute of Metal Research, Chinese Academy of Sciences, Shenyang 110016, China
[b] School of Materials Science and Engineering, University of Science and Technology of China, Shenyang 110016, China
[c] CAS Key Laboratory of Mechanical Behavior and Design of Materials, Department of Modern Mechanics, CAS Center for Excellence in Complex System Mechanics, University of Science and Technology of China, Hefei 230027, China

ARTICLE INFO

Article history:
Received 20 January 2021
Revised 29 March 2021
Accepted 23 April 2021
Available online 9 May 2021

Keywords:
Gradient nanotwinned Cu
Work hardening discrepancy
Extra strengthening
Strain delocalization
Elastic-plastic transition

ABSTRACT

This study investigates the mechanical behaviors of sandwiched gradient nanotwinned (GNT) Cu designed by only changing the soft component in the central layer with a fixed hard component at its surface. We found that as the work hardening discrepancy of components increases, both the strengthening and work hardening of GNT Cu increase simultaneously, producing a better strength-ductility synergy compared to their freestanding components. The optimized mechanical properties are results of the promoted strain delocalization, prolonged elastic-plastic transition, and larger strain gradient, which induces more geometrically necessary dislocations (GNDs) at the interfaces.

Gradient nanostructured (GNS) metallic materials [1] with spatially gradient microstructures ranging from nanometers to micrometers have attracted extensive attentions due to their superior mechanical properties such as high strength [2], good ductility [3–6], and considerable work hardening [2,7,8] compared to their counterparts with homogeneous and/or randomly mixed structures.

Generally, this built-in structural gradient is regarded to mainly depend on the difference of either yield strength or hardness between the different components. According to the existing strain gradient plasticity theory [9–11], the plastic strain gradient and progressive plastic yielding (due to the strength difference) of gradient microstructures are accompanied with the emitting and accumulation of dislocations, especially the geometrically necessary dislocations (GNDs) [9,12–14], resulting in an extra strengthening and work hardening [15–18]. For example, hardness gradient [2] or strength gradient [19] is quantitatively characterized as structural gradient in gradient nanotwinned (GNT) Cu samples with different gradient distributions of nanoscale twin thicknesses. Studies [2,19] showed that a concomitant increase in hardness/strength gradient is often accompanied by a marked increase in strength and work hardening. In particular, typical bundles of concentrated dislocations (BCDs) along the gradient direction form to suppress the strain/stress localization in the grain interiors. These BCDs contribute to ideal large plastic strains of GNT Cu.

As a matter of fact, besides the hardness/strength discrepancy, components in GNS metals also vary greatly in ductility; and more importantly, ductility and strength generally inversely behave [2,7]. The co-deformation of gradient structure depends greatly on both strength and ductility. To some extent, work hardening builds a bridge for both strength and ductility of materials [20]. However, the effect of work hardening discrepancy, which could represent the plastic incompatibility between components, on the deformation behaviors and strengthening mechanism of GNS metals is still unknown.

In this study, a series of two-components sandwiched GNT Cu, which have a fixed hard component on the surface while the soft central components changed with different work hardening abilities, are designed and fabricated under good control. The effect of work hardening discrepancy on tensile properties, elastic-to-plastic transitions, as well as deformation mechanisms are clarified.

As reported in the previous study [2], four individual homogenous nanotwinned (HNT) Cu are fabricated using direct-current electrodeposition and keeping the electrolyte temperatures at 20, 25, 30, and 35 °C, respectively. These samples are referred to as HNT-Ⓐ, Ⓑ, Ⓒ, and Ⓓ. Taking the four HNT structures as basic

* Corresponding author.
E-mail address: llu@imr.ac.cn (L. Lu).

[1] These authors contributed equally to this work.

[2] Lei Lu was an Editor of the journal during the review period of the article. To avoid a conflict of interest, Lei Lu was blinded to the record and another editor processed this manuscript.

https://doi.org/10.1016/j.scriptamat.2021.113975
1359-6462/

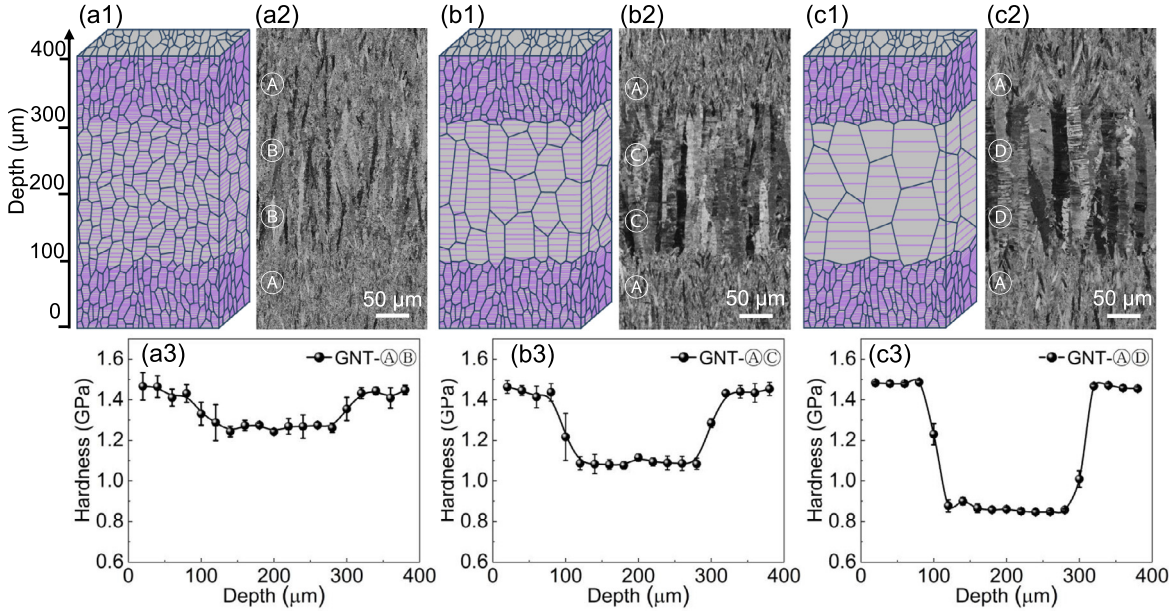

Fig. 1. The microstructure of three sandwiched GNT Cu samples. The schematic, SEM image and cross-sectional hardness distribution of GNT-ⒶⒷ (a1-a3), GNT-ⒶⒸ (b1-b3) and GNT-ⒶⒹ (c1-c3).

components, the three GNT Cu samples GNT-ⒶⒷ, GNT-ⒶⒸ and GNT-ⒶⒹ as illustrated by the schematics in Fig. 1 have spatial components stacking of ⒶⒷⒷⒶ, ⒶⒸⒸⒶ and ⒶⒹⒹⒶ, respectively. The surface components are all Ⓐ but the central component changes from Ⓑ to Ⓓ. In the three GNT Cu samples, each component has the same volume fraction (50%) and the total sample thickness keeps at ~ 400 μm.

The cross-sectional microstructures were characterized via a FEI Nova NanoSEM 460 field emission gun scanning electron microscope (SEM) using backscattering electron imaging (BSE). Kernel average misorientation (KAM) mapping was measured by electron backscatter diffraction (EBSD) under a voltage of 20 kV with a step size of 100 nm. The recorded data was analyzed with Oxford HKL channel 5 software. The most common approach used to distinguish the GND and SSD is that GNDs induce a local misorientation but SSDs can't. Based on this, the GND density can be estimated by the algorithm ($\rho_{GND} = 2\theta/(\mu b)$ [21], where θ is the local misorientation, μ is the unit length and b is the Burgers vector of dislocations).

The hardness distribution of GNT Cu samples along the depth were measured on a Qness Q10 A+ microhardness tester with a load of 50 g and dwell time of 10 s. Dog bone-shaped flat tensile specimens with a gauge length of 5 mm and a width of 2 mm were cut from the as-deposited GNT Cu sheets using electric spark machine and then mechanically and electrochemically polished. Uniaxial quasi static tensile tests were performed on an Instron 5848 microtester at a strain rate of 5×10^{-3} s^{-1} at ambient temperature. At least five tensile specimens were tested for each GNT Cu to ensure the data reproducibility. The strain of the gauge section was measured by a contactless MTS LX300 laser extensometer.

A full-field strain technique based on digital image correlation (DIC) was applied to detect the strain distribution on top and lateral surfaces of GNT Cu during tensile tests. Before DIC tests, random black and white speckle pattern was prepared by spraying black ink on a white surface as background. The strain distribution was analyzed using VIC-2D system with a resolution of 2.9 μm/pixel.

Cross-sectional SEM images of the three as-deposited GNT Cu samples are shown in Fig. 1. The typical microstructure of HNT Cu consists of preferentially oriented nano-meter twin lamellae, which are embedded within micro-meter columnar-shaped grains [2]. From component Ⓐ to Ⓓ, average grain size increases from 2.5 to 15.8 μm and average twin thickness increases from 29 to 72 nm. As shown in Figs. 1a1 and 1a2, GNT-ⒶⒷ consists of two Ⓐ components sandwiching a Ⓑ central layer. The hardness of Ⓑ (1.3 GPa) is lower than that of surface Ⓐ (1.5 GPa) (Fig. 1a3). GNT-ⒶⒸ (Figs. 1b1-b3) and GNT-ⒶⒹ (Figs. 1c1-c3) have a similar gradient structures but their centers are replaced by softer component Ⓒ and Ⓓ with hardness of 1.1 GPa and 0.8 GPa, respectively. No sharp interfaces but gradient transition between components in all three GNT Cu samples are formed, which might result from the epitaxial growth during electrodeposition [22].

Table 1
Tensile properties of GNT samples measured in the experiments (Exp.) and predicted by rule of mixture (ROM). σ_y, yield strength; σ_{uts}, ultimate tensile strength; δ_u, uniform elongation; $\Delta\sigma$, extra strengthening; $\varepsilon_{e\text{-}p}$, the ending strain of elastic-plastic transition.

Sample		σ_y (MPa)	σ_{uts} (MPa)	δ_u (%)	$\varepsilon_{e\text{-}p}$ (%)	$\Delta\sigma$ (%)
GNT-ⒶⒷ	Exp.	435 ± 10	464 ± 11	4.3 ± 1.1	0.9	3.6
	ROM	420 ± 16	445 ± 16	3.4 ± 0.6	1.3 (Ⓑ)	
GNT-ⒶⒸ	Exp.	400 ± 4	431 ± 5	6.6 ± 0.3	1.4	3.9
	ROM	385 ± 14	410 ± 18	4.8 ± 0.5	0.9 (Ⓒ)	
GNT-ⒶⒹ	Exp.	366 ± 11	410 ± 2	10 ± 0.9	1.7	9.6
	ROM	334 ± 19	371 ± 15	8.6 ± 1.2	0.6 (Ⓓ)	

Fig. 2a shows the tensile engineering stress-strain curves of the three GNT Cu samples in comparison to their homogenous freestanding counterparts HNT-Ⓐ, Ⓑ, Ⓒ and Ⓓ. As for HNT Cu, the yield strength substantially increases from 223 MPa to 446 MPa, but the ductility decreases from 22% to 1% from HNT-Ⓓ to HNT-Ⓐ, which results from the decreasing twin thickness and grain size [23]. With respect to HNT-Ⓐ, GNT-ⒶⒷ possesses a comparable yield strength (435 MPa) but a better uniform elongation (3%). The yield strength, ultimate tensile strength and uniform elongation of the three GNT Cu samples are summarized in Table 1. Based on the yield strengths of those four freestanding HNT components, the simple rule-of-mixture (ROM) [24] estimates of the yield strength of the GNT Cu are also included in Table 1. To quantitatively eval-

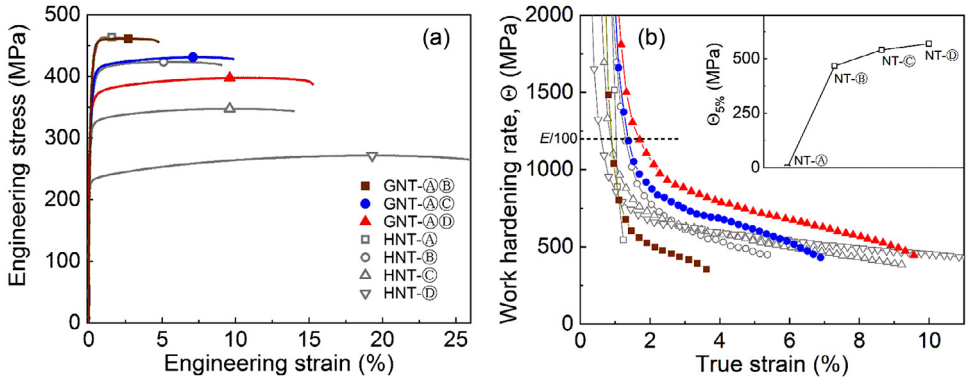

Fig. 2. Engineering stress-strain curves (a) and work hardening rate, Θ, vs. true strain curves (b) of GNT-ⒶⒷ, GNT-ⒶⒸ and GNT-ⒶⒹ in comparison to their HNT components. The inset of (b) shows the work hardening rates at a true strain of 5% of HNT Cu. The endings of elastic-plastic transition are indicated by the intersections of work hardening curves with the dash line at $\Theta = E/100$ in (b), where E is Young's modulus (120 GPa).

uate the strengthening of GNT structures, an extra strengthening parameter, $\Delta\sigma$, is defined as follows:

$$\Delta\sigma = \frac{\sigma_y - \sigma_{\mathrm{ROM}}}{\sigma_{\mathrm{ROM}}} \quad (1)$$

where σ_y is the measured yield strength and σ_{ROM} is the estimated strength by ROM. As expected, all GNT Cu exhibit extra strengthening behaviors relative to the HNT samples. The extra strengthening increases from 3.6% to 9.6% as for GNT-ⒶⒷ to GNT-ⒶⒹ.

Work hardening rate curves of both HNT and GNT Cu samples are shown in Fig. 2b. Obviously, we see two typical work hardening stages: the elastic-plastic transition stage with a steep decrease at small strain (less than ~2%) and the steady-state stage with a gentle decrease at larger stain. Compared to other HNT Cu samples, HNT-Ⓐ has no obvious steady-state work hardening stage. According to the description of work hardening stage in [20], the elastic to plastic transition stage of ploy-crystalline metals can be characterized by the work hardening rate Θ of $E/25$ to $E/100$. Here we choose the lower limit value ($E/100$) to define the ending strain of elastic-plastic stage, $\varepsilon_{e\text{-}p}$. The $\varepsilon_{e\text{-}p}$ of HNT and GNT Cu samples are presented in Fig. 2 and Table 1. From HNT-Ⓑ to HNT-Ⓓ, $\varepsilon_{\mathrm{e\text{-}p}}$ decreases from 1.3% to 0.6% while the work hardening ability at large strain increases. From the inset in Fig. 2b, the work hardening rate at a true strain of 5% increases from 0 to 568 MPa for HNT-Ⓐ to HNT-Ⓓ, which indicates the vast work hardening discrepancy among different components.

The work hardening behaviors of GNT Cu samples are uniquely related to HNT Cu samples, as shown in Fig. 2b. The work hardening curve with $\varepsilon_{\mathrm{e\text{-}p}} = 0.9\%$ of GNT-ⒶⒷ lies between HNT-Ⓐ and HNT-Ⓑ. Interestingly, $\varepsilon_{\mathrm{e\text{-}p}}$ increases to 1.4% (higher than that of HNT-Ⓒ) of GNT-ⒶⒸ and up to 1.7% (even higher than that of HNT-Ⓓ) of GNT-ⒶⒹ. More importantly, the work hardening rates of GNT-ⒶⒸ and ⒶⒹ are still higher than those of their soft central components at large strain stage. The above experimental results clearly show that a larger work hardening discrepancy between the two components results in a stronger extra strengthening and a higher work hardening in GNT structures.

To understand the effect of work hardening discrepancy on strengthening and work hardening of GNT Cu, we performed in-situ strain distribution DIC experiments on both top and lateral surfaces of GNT Cu samples, as presented in Figs. 3 and 4. Fig. 3a illustrates the distribution of tensile strain ε_{x} on the top surface of GNT Cu. As for GNT-ⒶⒷ (Figs. 3b1-b3), the strain distribution is quite uniform at a small strain ($\varepsilon_{\mathrm{app}} = 0.5\%$); but at $\varepsilon_{\mathrm{app}} = 2\%$, the strain distribution becomes heterogeneous, and a severe strain concentration (> 3%) is detected at a small region in the gauge section. As the applied strain increases up to 4%, strain localization is further intensified. The strain localization of GNT-ⒶⒸ is much alleviated compared to that of GNT-ⒶⒷ. Interestingly, the strain localization in GNT-ⒶⒹ is almost disappeared at $\varepsilon_{\mathrm{app}} = 4\%$, as shown in Figs. 3d1-d3. The results suggest that the strain localization of GNT Cu is effectively suppressed by a larger work hardening discrepancy between components.

Fig. 4a shows similar strain distributions on the lateral surfaces of the three GNT Cu samples. Considering the gradient plastic deformation accompanied with progressively yielding from soft to hard components, we choose a small strain at $\varepsilon = 1\%$ to study the strain distributions. No obvious difference of strain along sample thickness, ε_z, between surface and center can be detected in GNT-ⒶⒷ or GNT-ⒶⒸ. By contrast, it can be seen that ε_z of center is much larger than that of surface in GNT-ⒶⒹ. To further quantitatively evaluate the strain distribution, the average ε_z profiles are shown in Fig. 4b. For three GNT Cu samples, ε_z is larger in center than that at its surface, originating from the larger tensile plastic strain of center (due to the lower yield strength) with a larger plastic Poisson's ratio (~0.5) [25]. From GNT-ⒶⒷ to GNT-ⒶⒹ, the difference of ε_z between surface and central or the strain gradient of the whole sample increases substantially, also consistent with the larger yield strength difference.

Physically, the strain gradient in heterogenous structure needs GNDs to accommodate the incompatibility of plastic deformation [9–11]. As reported in 4-components GNT Cu samples in [2], extra BCDs as potential GND configurations are formed to accommodate the gradient deformation. However, the sandwiched GNT Cu samples in this study are almost BCDs free, even in GNT-ⒶⒹ with the largest strain gradient, as shown in Fig. 4c. This is possibly because the structural gradients of these sandwiched GNT Cu sample are insufficiently large, comparing to that of 4-components GNT Cu in [2].

Still taking the GNT-ⒶⒹ as example, we measured the GNDs distribution across the interface between Ⓐ and Ⓓ components by means of EBSD, as shown in Fig. 4d. The distribution of GND density reaches a peak at the interface, which is consistent with the gradient transition region in Fig. 1c. The GND density of Ⓐ (with smaller twin thickness and grain size) is higher than that of Ⓓ, due to more grain boundaries and twin boundaries emitting and accumulating the GNDs [9]. The GND density gradient and peak in the sandwiched GNT Cu are consistent with the results in the heterogenous Cu/bronze laminates [26], where GNDs pile up near the interface-affected zone (IAZ).

The above experimental results clearly indicate that work hardening discrepancy between components has a significant influence in the strengthening effect and deformation behaviors of GNT Cu samples. The strain localization of GNT Cu can be effectively sup-

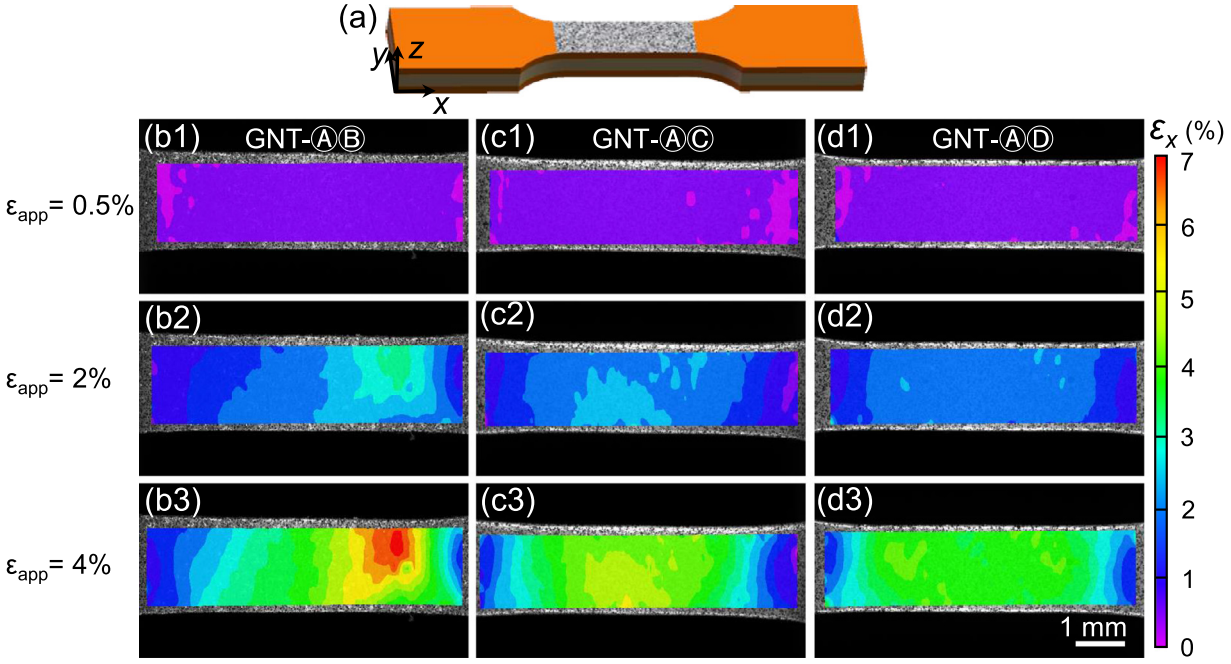

Fig. 3. (a) Illustrates measurement of strain distribution on top surfaces of GNT Cu. The distribution of tensile strain, ε_x, on surface of GNT-ⒶⒷ (b1-b3), GNT-ⒶⒸ (c1-c3) and GNT-ⒶⒹ (d1-d3) at different applied tensile strains, ε_{app}.

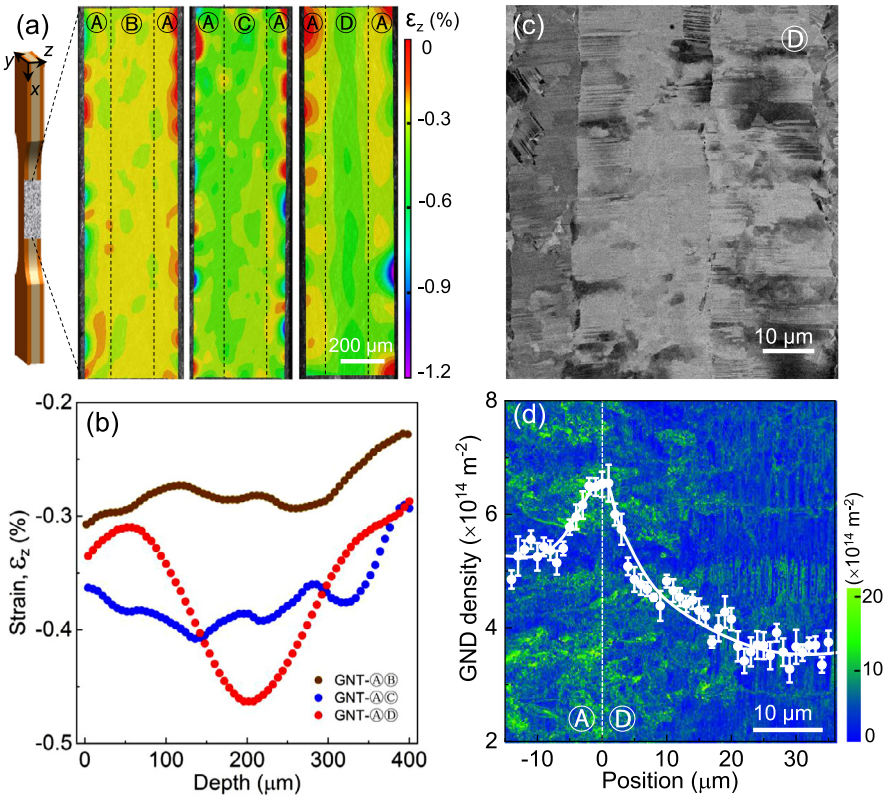

Fig. 4. Local strain distribution mapping on lateral surface (a) and corresponding profiles of average local lateral strain, ε_z, (b) of GNT-ⒶⒷ, GNT-ⒶⒸ and GNT-ⒶⒹ at $\varepsilon_{app} = 1\%$. (c) SEM image of Ⓓ in GNT-ⒶⒹ at $\varepsilon_{app} = 1\%$. (d) GND density mapping and average GND density variation across the interface of GNT-ⒶⒹ at $\varepsilon_{app} = 1\%$.

pressed not only in the elastic-plastic transition stage but also in the plastic deformation stage by increasing work hardening discrepancy. For HNT Cu samples, the elastic to plastic transition is undertaken from soft grains (with favorable orientations) to hard grains. However, in GNT Cu, the additional elastic-plastic transition is sustained by the progressive yielding from soft components (Ⓑ, Ⓒ or Ⓓ) to hard component (Ⓐ), indicating the hard component Ⓐ determines $\varepsilon_{e\text{-}p}$. Component Ⓐ has a limited ductility in free-standing sate, corresponding to the early strain localization or premature necking [27,28], but has a larger uniform elongation due to the alleviated strain localization when stacked in GNT structure. The strain delocalization can also be understood in terms of the

constraint between two components: the high work hardening capacity of soft component compensates for that of the hard component to keep the overall GNT Cu sample more stable and the GNDs at interface provide additional work hardening [16,26].

As shown in Figs. 2(b) and 3, the larger work hardening discrepancy increasingly suppresses the strain localization and improves the deformation stability. The suppressed strain localization in GNT structure can promote hard component Ⓐ to undertake higher stress, which accordingly enhances yield strength of GNT Cu and prolongs the elastic to plastic transition at initial deformation stage. Such suppressed strain localization and damage accumulation are beneficial to the GNDs induced strengthening [29] and the superior fatigue resistance, as observed in gradient nanostructured metals under cyclic loading [30,31], compared to its homogeneous counterparts.

In summary, we designed a series of gradient nanotwinned Cu with varying work hardening discrepancy and investigated their mechanical properties. An important insight from this study shows, for the first time, that as the work hardening discrepancy increases, the strengthening and work hardening of GNT Cu increase simultaneously with promoted strain delocalization. This finding provides an additional strategy to develop high-performance GNS metals.

Declaration of Competing Interest

The authors declare that they have no known competing financial interests or personal relationships that could have appeared to influence the work reported in this paper.

Acknowledgments

The authors acknowledge financial support by National Natural Science Foundation of China (NSFC, Grant Numbers. U1608257 and 51931010), the Key Research Program of Frontier Science and International partnership program (Grant Number. GJHZ2029), CAS, and LiaoNing Revitalization Talents Program (Grant Number. XLYC1802026). Z.C. acknowledges support by Project Funded by National Natural Science Foundation of China (NSFC, Grant Number. 52001312) and China Postdoctoral Science Foundation (Grant Number. BX20190336 and 2019M661150).

References

[1] X. Li, L. Lu, J. Li, X. Zhang, H. Gao, Nat. Rev. Mater. 5 (2020) 706–723.
[2] Z. Cheng, H.F. Zhou, Q.H. Lu, H.J. Gao, L. Lu, Science 362 (6414) (2018) 559 -+.
[3] T.H. Fang, W.L. Li, N.R. Tao, K. Lu, Science 331 (6024) (2011) 1587–1590.
[4] Y. Lin, J. Pan, H.F. Zhou, H.J. Gao, Y. Li, Acta Mater 153 (2018) 279–289.
[5] A. Jérusalem, W. Dickson, M.J. Pérez-Martín, M. Dao, J. Lu, F. Gálvez, Scr. Mater. 69 (11-12) (2013) 773–776.
[6] H.T. Wang, N.R. Tao, K. Lu, Scr. Mater. 68 (1) (2013) 22–27.
[7] X. Wu, P. Jiang, L. Chen, F. Yuan, Y.T. Zhu, Proc. Natl. Acad. Sci. U. S. A. 111 (20) (2014) 7197–7201.
[8] C.W. Shao, P. Zhang, Y.K. Zhu, Z.J. Zhang, Y.Z. Tian, Z.F. Zhang, Acta Mater 145 (2018) 413–428.
[9] M.F. Ashby, Philos. Mag. 21 (170) (1970) 399–424.
[10] N.A. Fleck, G.M. Muller, M.F. Ashby, J.W. Hutchinson, Acta Metall. Mater. 42 (2) (1994) 475–7487.
[11] H. Gao, Y. Huang, W.D. Nix, J.W. Hutchinson, J. Mech. Phys. Solids 47 (6) (1999) 1239–1263.
[12] Z. Zeng, X. Li, D. Xu, L. Lu, H. Gao, T. Zhu, Extreme Mech. Lett. 8 (2016) 213–219.
[13] L.P. Kubin, A. Mortensen, Scr. Mater. 48 (2002) 119–125.
[14] H. Gao, Y. Huang, Scr. Mater. 48 (2) (2003) 113–118.
[15] Y. Zhu, X. Wu, Mater. Res. Lett. 7 (10) (2019) 393–398.
[16] N.A. Fleck, M.F. Ashby, J.W. Hutchinson, Scr. Mater. 48 (2) (2003) 179–183.
[17] C.W. Sinclair, G. Saada, J.D. Embury, Philos. Mag. 86 (25-26) (2006) 4081–4098.
[18] Y.F. Wang, C.X. Huang, M.S. Wang, Y.S. Li, Y.T. Zhu, Scr. Mater. 150 (2018) 22–25.
[19] Y. Zhang, Z. Cheng, L. Lu, T. Zhu, J. Mech. Phys. Solids 140 (2020) 103946.
[20] U.F. Kocks, H. Mecking, Prog. Mater. Sci. 48 (3) (2003) 171–273.
[21] X. Ma, C. Huang, J. Moering, M. Ruppert, H.W. Höppel, M. Göken, J. Narayan, Y. Zhu, Acta Mater 116 (2016) 43–52.
[22] E. Chassaing, R. Wiart, Electrochim. Acta 29 (1984) 649–660.
[23] Z.S. You, L. Lu, K. Lu, Acta Mater. 59 (18) (2011) 6927–6937.
[24] S.L. Semiatin, H.R. Piehler, Metall. Trans. A 10 (1) (1979) 85–96.
[25] C.W. Bert, E.J. Mills, W.S. Hyler, J. Basic Eng. 89 (1) (1967) 35–39.
[26] C.X. Huang, Y.F. Wang, X.L. Ma, S. Yin, H.W. Höppel, M. Göken, X.L. Wu, H.J. Gao, Y.T. Zhu, Mater. Today 21 (7) (2018) 713–791.
[27] F. Yuan, D. Yan, J. Sun, L. Zhou, Y. Zhu, X. Wu, Mater. Res. Lett. 7 (1) (2019) 12–17.
[28] M. Goto, S.Z. Han, J. Kitamura, T. Yakushiji, J.H. Ahn, S.S. Kim, M. Baba, T. Yamamoto, J. Lee, Int. J. Fatigue 73 (2015) 98–109.
[29] Y. Wang, C. Huang, Z. Li, X. Fang, M. Wang, Q. He, F. Guo, Y. Zhu, Extreme Mech. Lett. 37 (2020) 100686.
[30] L. Yang, N.R. Tao, K. Lu, L. Lu, Scr. Mater. 68 (10) (2013) 801–804.
[31] J. Long, Q. Pan, N. Tao, M. Dao, S. Suresh, L. Lu, Acta Mater. 166 (2019) 56–66.